13 nm high-efficiency nickel-germanium soft x-ray zone plates

Julia Reinspach,[a] Magnus Lindblom, Michael Bertilson, Olov von Hofsten, Hans M. Hertz, and Anders Holmberg
Biomedical and X-Ray Physics, Department of Applied Physics, Royal Institute of Technology, 10691 Stockholm, Sweden

(Received 20 August 2010; accepted 26 September 2010; published 5 January 2011)

Zone plates are used as objectives for high-resolution x-ray microscopy. Both high resolution and high diffraction efficiency are crucial parameters for the performance of the lens. In this article, the authors demonstrate the fabrication of high-resolution soft x-ray zone plates with improved diffraction efficiency by combining a nanofabrication process for high resolution with a process for high diffraction efficiency. High-resolution Ni zone plates are fabricated by applying cold development of electron-beam-patterned ZEP 7000 in a trilayer-resist process combined with Ni-electroplating. High-diffraction-efficiency Ni–Ge zone plates are realized by fabricating the Ni zone plate on a Ge film and then using the finished zone plate as etch mask for anisotropic CHF_3 reactive ion etching into the underlying Ge, resulting in a Ni–Ge zone plate with improved aspect ratio and zone plate efficiency. Ni–Ge zone plates with 13 nm outermost zone width composed of 35 nm Ni on top of 45 nm Ge were fabricated. For comparable Ni and Ni–Ge zone plates with an outermost zone width of 15 nm, the diffraction efficiency was measured to be 2.4% and 4.3%, respectively, i.e., an enhancement of a factor of 2. © *2011 American Vacuum Society.*
[DOI: 10.1116/1.3520457]

I. INTRODUCTION

Nanoimaging methods in the soft x-ray regime are presently developing rapidly. One example is water-window (2–4 nm wavelength) x-ray microscopy with applications in biology, environmental science, and magnetic studies.[1,2] For very high spatial resolution soft x-ray imaging, the optics of choice are zone plates, where the resolution is determined by the outer zone widths. In the present article, we show that the efficiency of soft x-ray zone plates with state-of-the-art resolution can be enhanced by fabricating Ni–Ge compound zones.

Zone plate lenses are circular diffraction gratings with alternating transparent and opaque (and/or phase shifting) zones. The period of these zones decreases from the center to the outer part. The width of the outermost zone, dr_N, is a critical parameter since the achievable resolution in imaging is proportional to this number.[1] The outermost zone width is limited by fabrication issues. Today, soft x-ray zone plates with $dr_N = 25-50$ nm are routinely fabricated,[3–5] while outer zone widths as small as 12 and 13 nm have been recently reported.[6,7] Another important parameter is the diffraction efficiency, i.e., the fraction of incoming x-ray flux that is diffracted into a certain diffraction order by the zone plate. Usually, the first diffraction order is used for imaging as most of the x-ray photons are diffracted into this order. High diffraction efficiency is important since it reduces the necessary exposure time to achieve a sufficient signal-to-noise ratio in the x-ray images. Furthermore, in many applications, a short exposure time also makes the imaging less sensitive to thermal and mechanical drift, and vibrations. The diffraction efficiency primarily depends on the x-ray wavelength, the height of the zones, and the zone material, but also on factors such as line-edge roughness and line-to-space (L:S) ratio.[8] For water-window wavelengths, Ni, Ge, and Au are commonly used as x-ray optical materials since their absorption and/or phase shift properties result in high efficiency. Figure 1(a) shows the first-order diffraction efficiency for Ni at $\lambda = 2.88$ nm plotted as a function of zone height and for different L:S ratios. The calculations follow Ref. 8. The maximum efficiency is obtained for a Ni height of ~200 nm and a 1:1 L:S ratio. However, in practice, nanofabrication issues limit the achievable aspect ratio and, thus, real zone plates typically have lower heights. This is especially true for zone plates with very small outermost zone widths. For example, for the 12 and 13 nm zone plates,[6,7] the electroplated Au and Ni are 30 and 35 nm, respectively. Consequently, the diffraction efficiency is low [see Fig. 1(a)].

Here, we describe a method to enhance the efficiency of 15 and 13 nm soft x-ray zone plates. Similar to previously demonstrated 30 nm Ni–Ge zone plates, a Ni zone plate is fabricated on top of a Ge film.[9] The Ni is then used as hard-mask in a subsequent dry etch of the Ge, producing high Ni–Ge compound zones and a higher efficiency. The theoretical efficiency enhancement is shown in Fig. 1(b). In the present article, we extend this method to the smallest zone widths by combining it with our cold development process[7,10] for the fabrication of narrow-line-width Ni zone plates. We show that the Ge can be etched with sufficient depth and uniformity to result in 13 nm Ni–Ge zone plates with an outer zone width height of 80 nm, resulting in a diffraction efficiency that is almost a factor of 2 better than the efficiency of the corresponding Ni zone plate [see Fig.

[a]Electronic mail: julia.reinspach@biox.kth.se

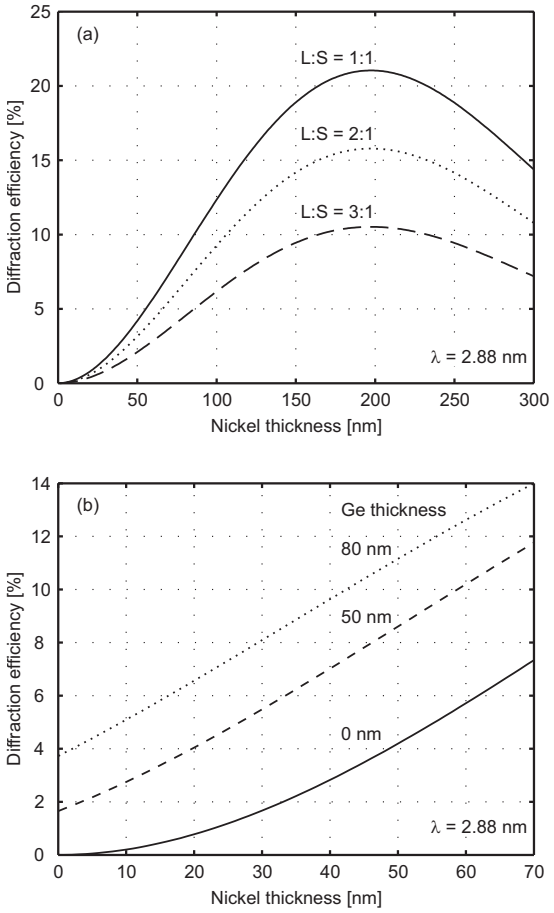

FIG. 1. Grating efficiency as a function of Ni height for $\lambda = 2.88$ nm. In (a), the efficiency is plotted as a function of Ni height and for different L:S ratios. Optimal values are obtained for a Ni thickness of ~200 nm. (b) The efficiency for Ni–Ge gratings for a Ge layer of 0 (i.e., Ni only), 50, and 80 nm.

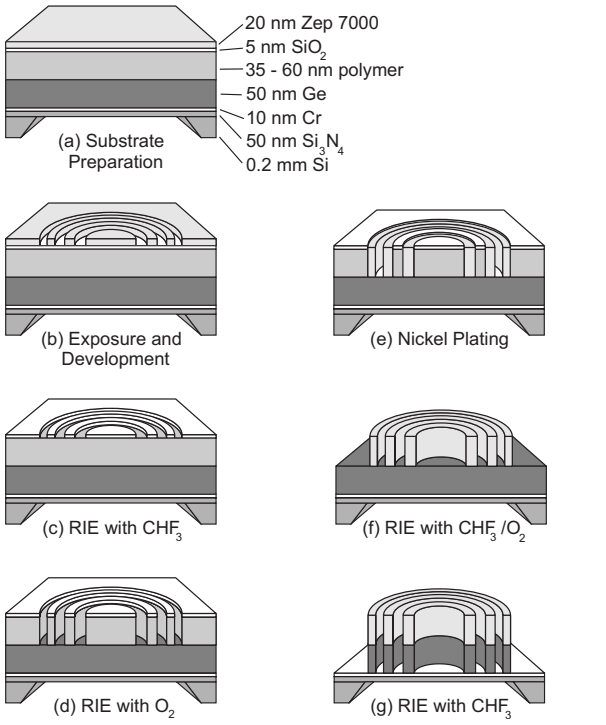

FIG. 2. Fabrication process for Ni–Ge zone plates. The trilayer stack is structured by electron beam lithography and RIE, followed by Ni electroplating. The Ni is then used as hardmask for RIE into the underlying Ge layer.

1(b)]. For Ni–Ge zone plates with $dr_N = 15$ nm and a total height of 105 nm, the efficiency enhancement was also experimentally verified.

II. NANOFABRICATION

In the following two sections, we describe and evaluate the fabrication process.

A. Fabrication process

The fabrication process is outlined in Fig. 2. In summary, a Ni zone plate is first fabricated by electroplating into a mold made from a trilayer resist[11] on top of a thick Ge layer [Figs. 2(a)–2(f)]. The pattern is then extended into the Ge layer by dry etching using the Ni zone plate as mask [Fig. 2(g)]. The trilayer resist was chosen in order to obtain the highest possible resolution with a high aspect ratio. A single-layer resist has also been tested but without reaching the same combination of resolution and aspect ratio.

A material stack was first prepared on commercially available 50 nm thick Si_3N_4-membrane substrates (Silson Ltd.). The membranes are used since they have a high soft x-ray transmission. They were first coated with a 10 nm thick Cr etch stop and a 50 nm thick Ge layer. This coating also serves as the seed layer for the electroplating. Thereafter, the trilayer stack was deposited, consisting of 40 or 55 nm polymer plating mold (PI-2610, HD Microsystems), 5 nm SiO_2 hardmask, and 20 nm electron beam resist (ZEP 7000, Zeon Chemicals L.P.). The Cr and Ge layers were deposited by electron beam vapor deposition (Edwards Auto 306, 10^{-6} Torr base pressure) and the SiO_2 layer was sputter deposited (AJA Orion, 10^{-8} Torr base pressure). The PI-2610 and the ZEP 7000 layers were spincoated and subsequently baked in an oven. The PI-2610 was baked for 120 min at 350 °C and the ZEP 7000 for 30 min at 170 °C. After the substrate preparation, the ZEP 7000 was patterned by electron beam lithography (Raith 150 system) at 25 kV and at a dose of ~300 $\mu C/cm^2$. This dose is necessary for cold development processing since the sensitivity of the resist decreases with temperature and is about three times higher than the dose required for room temperature development.[7] The development was performed in hexylacetate for 30 s at −50 °C, followed by a rinse in isopropyl alcohol and in pentane. The pattern was then transferred to the SiO_2-layer by reactive ion etching (RIE) (Oxford Instruments, Plasmalab 100) with CHF_3 at the following parameters: 10 SCCM gas flow (SCCM denotes cubic centimeter per minute at STP), 10 mTorr pressure, 25 W sample RF power, and an etch time of 40 s. The SiO_2 served as hardmask for the subsequent O_2-RIE step (Oxford Instruments, Plasmalab 80+) into the polymer plating mold. This was performed at 10 SCCM gas flow, 50 W sample RF power, 3 mTorr pressure, and an etch

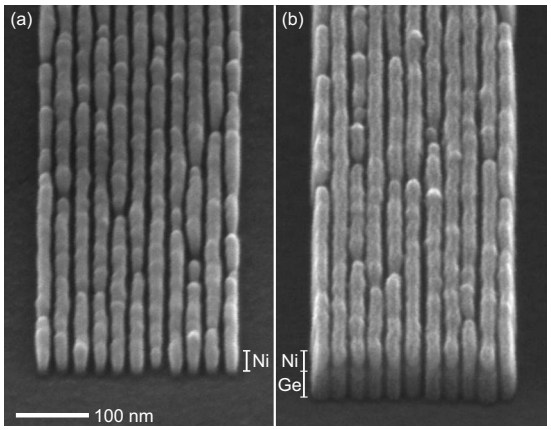

FIG. 3. SEM images of two 13-nm half-pitch Ni gratings (a) before and (b) after etch into the underlying Ge layer. Due to contamination of the Ge surface during SEM imaging, the images cannot be recorded on the same grating. The two gratings are from the same batch. The images are taken under a viewing angle of 52°.

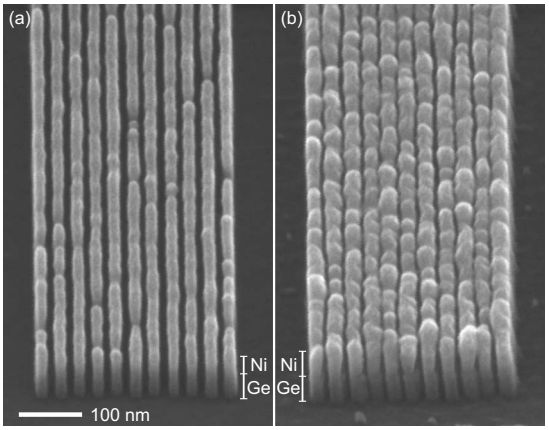

FIG. 4. Comparison between 15-nm half-pitch Ni–Ge gratings made from a mold of (a) 40 nm and (b) 55 nm height, respectively. The prolonged O_2 etch time, necessary for the thicker polymer layer, increases the undercut in the polymer and results in broader Ni lines after the electroplating. The broad lines are then also transferred into the Ge layer, giving an overall nonoptimal L:S ratio. The images are taken under a viewing angle of 52°.

time of 1–2 min, depending on the thickness of the polymer layer. The polymer mold was then filled with Ni by electroplating in a nickel sulfamate bath (Enthone, Inc., Lectro-Nic 10–03) at a temperature of 53 °C, a pH of 3.25, and a rate of 10–20 nm/min. Subsequently, the mold was removed by repeating the two RIE steps. At this step, the Ni zone plate is completed and only the etching into the underlying Ge layer remains. The Ge etch was carried out by RIE (Oxford Instruments, Plasmalab 100) with CHF_3 for 10 min etch time, 10 SCCM gas flow, 3 mTorr pressure, and 100 W sample RF power.

B. Process evaluation

Figures 3(a) and 3(b) show two comparable 13 nm gratings before and after the Ge etch step. The Ni and Ge thicknesses are 35 and 45 nm, respectively. Clearly, the aspect ratio is significantly improved by the Ge etch. Below, we discuss the process parameters that limit the resolution and aspect ratio in the present Ni–Ge process.

The highest resolution that can be fabricated in Ni–Ge structures depends on the achievable resolution in the Ni fabrication process. As previously shown, the cold development process can give 11-nm half-pitch lines in the resist.[7] This linewidth cannot, however, be transferred into Ni structures (and thus not into Ni–Ge structures) due to isotropic etching of the polymer plating mold. The isotropic etch results in an undercut to the SiO_2-hardmask, which damages the structures with the smallest linewidths. In addition, the undercut results in a poor L:S ratio of the electroplated Ni lines. The L:S ratio that is obtained for the Ni structures is therefore very dependent on the etch time and, hence, the mold thickness. In Fig. 4, the problem is illustrated by a comparison of 15-nm half-pitch Ni gratings that are made out from 40 and 55 nm high molds. The plated Ni heights were 35 and 55 nm, respectively, and the Ge height is 50 nm in both cases. The undercut to the hardmask and the resulting varying L:S ratio were not expected, since the recipe has given good anisotropy in >25 nm half-pitch structures. Obviously, the down scaling affects the etch profile. The used O_2 recipe parameters cannot easily be changed to reduce the isotropic effect. The chamber pressure is the lowest possible that gives a stable plasma in the etcher, and increasing RF power increases line-width loss of the hardmask. The conclusion is that the etch recipe must be changed so that a side-wall passivating film is formed. This could either be done by etching the polymer at cryogenic temperatures or adding a film-forming gas to the plasma.

The final Ge etch step made in the CHF_3 plasma has been reliable and the Ni structures are observed to be a good etch mask. The etch profile is anisotropic, but the etch rate is aspect ratio dependent. In large open areas, the etch rate is ~ 30 nm/min, while it decreases considerably as lines are made smaller. Typically, an etch time of 10 min has been used to clear the 13-nm half-pitch structures where the Ge thickness is 50 nm. Scanning electron microscopy (SEM)-inspection shows that some smoothening of the Ni top surface occurs during etch, but there is no line-width loss even during extended plasma etching. Any thickness loss is difficult to measure directly in the structures, but profilometer step-height measurements (Tencor, P15 system) performed in micrometer sized structures give an etch rate of ~ 0.3 nm/min under the given plasma conditions. Given this excellent durability of the Ni, and the anisotropic etch of the Ge, we are convinced that the thickness of the Ge layer can be increased further, leading to an increase in the diffraction efficiency of the zone plate.

In summary, we conclude that the process is suitable for structures down to 13 nm half-pitch and that the pattern extension into the Ge layer preserves the pattern quality of the Ni structures. Even if there is room for further improvements, in terms of L:S ratio and Ge height, the results immediately open up for the fabrication of Ni–Ge zone plates at this very high resolution. As shown in Fig. 1(b), such zone plates will have a significantly improved efficiency com-

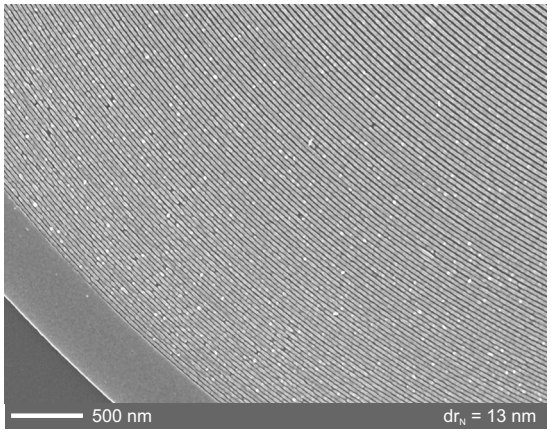

FIG. 5. Outermost part of a Ni–Ge zone plate with $dr_N=13$ nm. The zone plate is composed of 45 nm Ge and 35 nm Ni. The quality of the zone plate is uniform over the whole zone plate.

pared to present Ni zone plates. In the next section, high-resolution Ni–Ge zone plates are presented and characterized.

III. FABRICATED ZONE PLATES AND CHARACTERIZATION

We have fabricated zone plates with dr_N of 15 and of 13 nm. Figure 5 shows a SEM image of the outermost part of one of the fabricated zone plates with $dr_N=13$ nm. The diameter is 19 μm and the focal length is 86 μm at $\lambda=2.88$ nm. The Ni thickness is 35 nm and the Ge thickness is 45 nm, resulting in a total height of 80 nm. The zone plates with $dr_N=15$ nm have a diameter of 26 μm and a focal length of 135 μm at $\lambda=2.88$ nm. The total height is 105 nm, composed of 55 nm Ni on top of 50 nm Ge.

To experimentally verify the efficiency enhancement by the added Ge layer, a batch of zone plates in only Ni was prepared for comparison. They had the same focal length, diameter, and Ni thickness as the Ni–Ge zone plates. The only difference was that in the Ni zone plates, the Ge layer was reduced to 10 nm, which is needed as seed layer for electroplating. A laboratory laser-plasma-based arrangement was used to measure the first-order diffraction efficiency at $\lambda=2.88$ nm.[12] In this setup, the diffraction efficiency is determined by detecting the first diffraction order photon flux and comparing it with the photon flux of a calibrated reference signal. As reference signal, the zeroth order undiffracted beam was used. For the zone plates with $dr_N=15$ nm, the average measured efficiency was $2.4\pm0.3\%$ for the Ni zone plate and $4.3\pm0.3\%$ for the Ni–Ge zone plate. The uncertainty is the calculated standard deviation out of five measurements. The efficiencies presented here are the groove efficiencies, i.e., the absorption in the substrate and the plating base has been compensated for. The measured efficiencies are ~50% of the theoretical ones given by Fig. 1(b). The experimental results are in good agreement with theory when taking into account that ideal L:S ratio, line-edge roughness, and line profile are not easily achieved at those small scales. For comparison, Ni zone plates with $dr_N=25$ nm were measured to have ~70% of their theoretical diffraction efficiency.[12] The results obtained here show that the efficiency of a high-resolution soft x-ray zone plate is not limited by the best achievable aspect ratio of a Ni zone plate (in this case, ~55 nm for $dr_N=15$ nm), but can be significantly improved by an additional Ge dry etch step.

SEM inspection shows that the 13 nm Ni–Ge zone plates have the same quality as the 15 nm ones. Thus, we expect them to achieve at least the same factor of 2 efficiency enhancement as the 15 nm zone plates. Due to the very short focal length of the 13 nm zone plates, it was impossible to experimentally verify this in the present efficiency measurement arrangement. The setup will be improved for coming experiments to accommodate zone plates with shorter focal lengths.

IV. SUMMARY

In this article, we presented a process for the fabrication of high-resolution soft x-ray zone plates with improved diffraction efficiency. Zone plates with an outermost zone width dr_N down to 13 nm, consisting of 35 nm Ni and 45 nm Ge, were successfully fabricated. For zone plates with $dr_N=15$ nm, consisting of 55 nm Ni and 50 nm Ge, the efficiency enhancement compared to an equivalent 55 nm thick Ni zone plate was almost two times. The results agree well with theory.

ACKNOWLEDGMENTS

The authors gratefully acknowledge the financial support of the Swedish Science Research Council, the Swedish Foundation for Strategic Research, the Wallenberg Foundation, and the Göran Gustafsson Foundation.

[1] D. T. Attwood, *Soft X-Rays and Extreme Ultraviolet Radiation* (Cambridge University Press, Cambridge, 1999), pp. 337–394.
[2] C. David, F. Nolting, F. Pfeiffer, C. Quitmann, and M. Stampanoni, J. Phys.: Conf. Ser. **186** (2009).
[3] M. Peuker, Appl. Phys. Lett. **78**, 2208 (2001).
[4] S. J. Spector, C. J. Jacobsen, and D. M. Tennant, J. Vac. Sci. Technol. B **15**, 2872 (1997).
[5] M. Lindblom, J. Reinspach, O. von Hofsten, M. Bertilson, H. M. Hertz, and A. Holmberg, J. Vac. Sci. Technol. B **27**, L1 (2009).
[6] W. Chao, J. Kim, S. Rekawa, P. Fischer, and E. H. Anderson, Opt. Express **17**, 17669 (2009).
[7] J. Reinspach, M. Lindblom, O. von Hofsten, M. Bertilson, H. M. Hertz, and A. Holmberg, J. Vac. Sci. Technol. B **27**, 2593 (2009).
[8] J. Kirz, J. Opt. Soc. Am. **64**, 301 (1974).
[9] M. Lindblom, J. Reinspach, O. von Hofsten, M. Bertilson, H. M. Hertz, and A. Holmberg, J. Vac. Sci. Technol. B **27**, L5 (2009).
[10] J. Reinspach, M. Lindblom, O. von. Hofsten, M. Bertilson, H. M. Hertz, and A. Holmberg, Microelectron. Eng. **87**, 1583 (2010).
[11] A. Holmberg, S. Rehbein, and H. M. Hertz, Microelectron. Eng. **73–74**, 639 (2004).
[12] M. Bertilson, P. A. C. Takman, U. Vogt, A. Holmberg, and H. M. Hertz, Rev. Sci. Instrum. **78**, 026103 (2007).